RSC Advances

ROYAL SOCIETY OF CHEMISTRY

www.rsc.org/advances

A new strategy was developed to grow γ-Fe_2O_3 nanosheet arrays on the graphene sheets, showing excellent electromagnetic wave absorption property with lightweight characteristic.

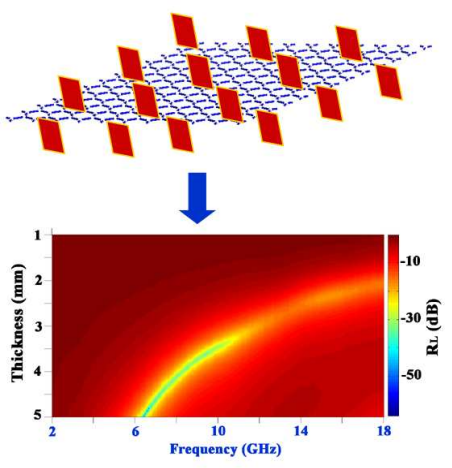

Cite this: DOI: 10.1039/c0xx00000x

www.rsc.org/xxxxxx

ARTICLE TYPE

Growth of γ-Fe_2O_3 nanosheet arrays on graphene for electromagnetic absorption applications†

Yulan Ren, [a] Chunling Zhu, *[a] Lihong Qi, [b] Hong Gao, [c] and Yujin Chen *[b]

Received (in XXX, XXX) Xth XXXXXXXXX 20XX, Accepted Xth XXXXXXXXX 20XX

DOI: 10.1039/b000000x

We developed a seed-assisted method to grow ultra-thin γ-Fe_2O_3 nanosheets with a paramagnetic behaviour on the surfaces of the graphene sheets. The scanning electron microscope and the transmission electron microscope measurements showed that the length, the height and the thickness of the nanosheets were about 140, 120 and 5 nm, respectively. The measured electromagnetic parameters indicated that the three-dimensional (3D) graphene/γ-Fe_2O_3 nanosheet arrays exibited significantly enhanced electromagnetic wave absorption property compared to that of the graphene sheets and some magnetic nanomaterials. The minimal reflection loss was less than −15.2 dB for 3D graphene/γ-Fe_2O_3 nanosheet arrays with the thicknesses of 2 mm, and it was up to −64.1 dB when the thickness was 4.92 mm. The good electromagnetic wave absorption properties of the 3D graphene/γ-Fe_2O_3 nanosheet arrays indicate that they are very promising for applicaton in electromagnetic wave absorbing field.

1 Introduction

Heteronanostructures have drawn the unique attention in the research field of nanoscience because it's simply difficult for the single component material to realize corresponding exceptional properties and multifunctionality. Graphene (G) has excellent mechanical, electrical, thermal, and optical properties together with an ultrathin effectively 2D structure. Furthermore, graphene can incorporate abundant oxygen functional groups such as −OH and −C=O on its surfaces. These properties make it an ideal substrate for the deposition and/or growth of other functional materials. Recently, various G-based heteronano structures have been fabricated extending the application of graphene into new fields, such as energy storage and conversion, chemical catalysts, and optoelectronic devices and sensors.[1–17]

Among these materials, magnetic graphene heteronanostructures have many potential applications as contrast enhancement agents in magnetic resonance imaging, energy storage, electromagnetic (EM) wave absorption, and so on.[4–13] For example, G/Fe_3O_4 heteronanostructures with superparamagnetic, conductive and multifunctional properties show great promise as materials for magnetic resonance imaging.[4] Very recently, highly ordered 3D G-based heteronanostructures with high specific surface area, a large number of active sites and superior mechanical strength have been synthesized. Because of their unique geometry, these 3D heteronanostructures are being considered for applications in optoelectronic devices, catalysts, and lithium ion batteries.[15, 17, 18] However, growtn of magnetic nanosheet arrays on the surfaces of the graphene sheets have rarely been reported.

EM wave-absorbing materials have attracted a great deal of attention because of increasing EM interference and radiation problems. For these applications, lightweight materials with strong absorption properties are required. To meet these requirements, researchers have recently developed various methods to fabricate nanostructures for use in lightweight EM absorbers.[19–31] Heteronanostructured materials exhibit strong EM absorption properties because of interfacial and synergistic effects. For example, the reflection losses for EM waves reached –25 dB for carbon nanotube/Fe core/shell nanostructures with a thickness of 1.2 mm, [21] and –30 dB for Fe_3O_4/ZnO core/shell nanorods with a thickness of 1.5mm.[27] However, the amount of the absorbers added to the paraffin matrix needs to be decreased significantly for practical applications.

Graphene, representative of a new class of 2D carbonaceous materials, is a very promising candidate for a lightweight EM absorber. However, its high conductivity, which would lead to its poor EM absorption ability is a serious drawback.[32–34] This drawback can be overcome to some extent by designing G-based heteronanostructures, in which dielectric or magnetic loss nanostructured materials are deposited on the surface of the graphene sheets.[6–12, 18] The fabrication of G-based heteronanostructures using a rational design process may be an efficient strategy for obtaining EM absorbers that are both lightweight and that have strong absorption properties.

Very recently, we developed a new seed-assisted method for fabricating a combination 3D G/SiO_2@Fe_3O_4 core/shell nanorod arrays architecture.[35] In this work, we fabricated 3D G/γ-Fe_2O_3 nanosheet array (NSA) heteronanostructures by a modification of the above method. Three process steps were involved in the formation of the 3D G/γ-Fe_2O_3 NSAs, as shown in Figure 1. The graphene sheets were first dispersed in a ferric nitrate aqueous solution to grow β-FeOOH nanostructures on their surfaces (step 1 in Figure 1).[6, 8] These nanostructures served as "seeds" for the growth of β-FeOOH NSAs on the surfaces of the graphene sheets

in a ferric chloride aqueous solution under a hydrothermal condition (step 2 in Figure 1). Finally, the 3D G/γ-Fe_2O_3 NSAs were obtained after a thermal treatment of the G/β-FeOOH NSAs (step 3 in Figure 1). Because of their special morphology, the 3D G/γ-Fe_2O_3 NSA heterostructures exhibited very good properties, including strong attenuation of EM waves and low device mass.

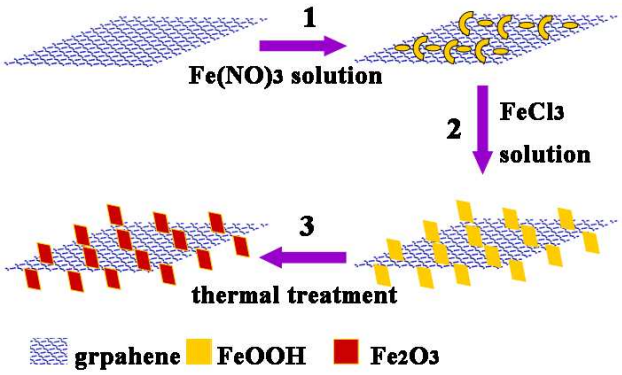

Figure 1 Growth processes of 3D G/γ-Fe_2O_3 NSAs.

2 Experimental section

2.1. Materials

The graphene sheets used in this work were purchased from Nanjing XFNano Material Tech Co., Ltd. (Nanjing City, China); its thickness and specific surface area are about 0.8 nm and 500-600 $m^2 \cdot g^{-1}$, respectively, and the corresponding oxygen content is about 7 wt%. Its synthesis is as follows: graphite oxide (GO) was prepared from natural graphite using a modified Hummers method. The GO was then thermally treated at a high temperature under an N_2 flow, and finally reduced at 1200°C under an H_2 atmosphere. All of other reagents were analytically pure, and used without further purification.

2.2. Synthesis of G/β-FeOOH NSAs

The 3D G/γ-Fe_2O_3 NSAs were fabricated by a seed-assisted method, as illustrated in Figure 1. 0.01 g of graphene sheet was dispersed into 300 mL water under ultrasonication, then 1.0 g of $Fe(NO_3)_3 \cdot 9H_2O$ was added. This mixture was stirred at 50°C for 2 h. The precipitates were separated by centrifugation, washed with distilled water and pure ethanol, then vacuum-dried. 15 mg of the precipitate was dispersed in 35 mL of a solution containing 0.5 g $FeCl_3 \cdot 6H_2O$ and 1.0 g sodium nitrate, and this mixture was stirred for 20 min. This mixture was then transferred into a Teflon-lined stainless steel autoclave with a capacity of 50 mL for hydrothermal treatment at 60°C for 12 h. After the autoclave cooled to room temperature naturally, the precipitates were separated by centrifugation, washed with distilled water and pure ethanol, and dried in air.

2.3. Synthesis of G/γ-Fe_2O_3 NSAs

The final G/γ-Fe_2O_3 NSAs were fabricated by thermal treatment of the G/β-FeOOH NSAs at 300°C for 2 h in air.

2.4 Structural Characterization

The morphology and size characteristics of the synthesized samples were characterized using a Hitachi S-5200 scanning electron microscope (SEM) and an FEI Tecnai-F20 transmission electron microscope (TEM) equipped with a Gatan imaging filter (GIF). The operating voltages of SEM and TEM were 5 and 200 kV, respectively. The crystal structure of the sample was determined by X-ray diffraction (XRD) using a Rigaku D/max 2550 V diffractometer and Cu Kα radiation. X-ray photoelectron spectroscopy (XPS) measurements were carried out using a PHI 5700 ESCA spectrometer with Al K□ radiation. The Raman spectrum was collected on a HR Jobin Yvon spectrometer. The magnetic properties of the hierarchical 3D G/γ-Fe_2O_3 NSA material were measured using vibrating sample magnetometry (VSM).

2.5. EM parameter measurements

The EM properties of the samples were measured using the transmission/refection coaxial line method. The measurement setup consisted of an ANRITSU 37269D vector network analyzer with a synthesized sweep oscillator source and an S–parameter test set. The measured samples were prepared by uniformly mixing 20 wt% of the sample in a paraffin matrix. The mixture was then pressed into toroidal samples (φ_{out}: 7.00 mm; φ_{in}: 3.04 mm).

3 Results and discussions

3.1. Growth of β-FeOOH seeds on the surfaces of the graphene sheets

It is well known that amorphous $Fe(OH)_3$ colloidal nanoparticles can be produced during the hydrolysis of ferric nitrate.[36, 37] If the template materials are dispersed in the ferric nitrate solution prior to hydrolysis, the colloid nanoparticles will be deposited on the template surfaces.[6, 8, 36–39] The hydrolysis conditions (time and temperature) and the type of template material have an influence on the morphology and crystalline phase of the final deposited product. For example, amorphous $Fe(OH)_3$ particles would be produced on the surface of α-MoO_3 nanorods at a hydrolysis temperature of 50 °C,[38, 39] whereas β-FeOOH nanocrystals would be formed on the surfaces of the graphene sheets under the same conditions.[6, 8, 40] Under the present experimental conditions, β-FeOOH nanostructures with different morphologies grow on the surfaces of the graphene sheets. As shown in Figure 2(a), aside from a few small nanoparticles, many nanosheets with a length of about 150 nm grew on the graphene. A typical low-resolution TEM image (Figure 2(b)) indicates that the diameters of the small β-FeOOH particles and the thicknesses of the β-FeOOH nanosheets are less than 5 nm and 8 nm, respectively. Distinct lattice fringes are observed in the high-resolution TEM (HRTEM) images (the insets in Figure 2(c) and (d)), suggesting that both the nanoparticles and the nanosheets are crystalline. Figure 2(e) shows the selected area electron diffraction (SAED) pattern of the composites. The labelled diffraction rings in the pattern correspond to the (200), (101), (301) and (600) planes of orthorhombic β-FeOOH (JCPDS card number 75–1594, cell parameters: a = 8.40 Å and c = 3.0 Å). These results reveal that β-FeOOH nanocrystals, including nanoparticles and nanosheets, have been grown on the surfaces of the graphene sheets.

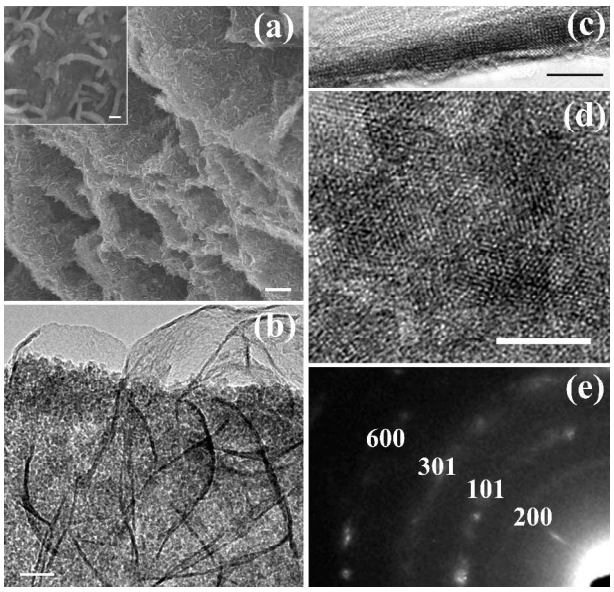

Figure 2 Structural characterizations of β-FeOOH seed/G composites. (a) SEM image, the inset shows a magnified SEM image, (b) TEM image, (c) HRTEM image for β-FeOOH nanosheets, (d) HRTEM image for β-FeOOH nanoparticles, and (e) SAED pattern.Scale bar: (a) 400 nm, and the inset images: 50 nm, (b) 20 nm, and (c) and (d) 5 nm.

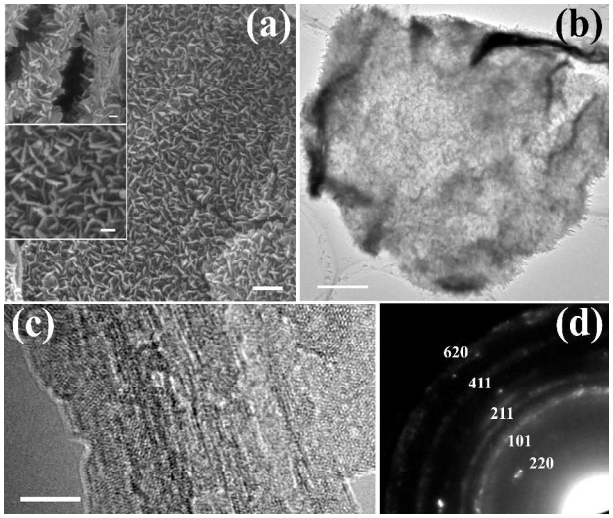

Figure 3 Structural characterizations of the G/β–FeOOH nanosheets arrays. (a) Top-view SEM image, up-inset showing cross-section SEM image, and bottom-inset showing magnified top-view SEM image, (b) low-resolution TEM image, (c) HRTEM image for an individual β–FeOOH nanosheet and (d) SAED pattern. Scale bar: (a) 400 nm, and the inset images: 100 nm, (b) 1 μm, and (c) 5 nm.

3.2. Formation of G/β-FeOOH NSAs

All of the indexed diffraction peaks in the XRD pattern collected from the G/β-FeOOH NSA materials can be assigned to orthorhombic β–FeOOH crystals(Figure S1, ESI). † Top-view SEM images, shown in Figure 3(a) and the bottom inset, indicate that most of the β-FeOOH nanosheets with a typical length of about 180 nm are grown on the surfaces of the graphene sheets. The cross-sectional SEM image (top inset in Figure 3(a)) clearly shows that β-FeOOH nanosheets with a height of about 130 nm grow on both sides of the graphene sheets, forming interesting 3D architectures. In the case where the β-FeOOH nanosheets are present on both side surfaces of graphene sheets, the efficient stacking and aggregation of individual graphene sheets is impaired.

The HRTEM image in Figure 3(c) demonstrates that the β-FeOOH nanosheets have poor crystallinity. The SAED pattern in Figure 3(d) confirms that β-FeOOH nanosheets are polycrystalline, and the labeled diffraction rings correspond to the (220), (101), (211), (411), and (620) crystalline planes of orthorhombic β-FeOOH. The β-FeOOH nanosheets grow more densely on the G surfaces that have been hydrothermally treated. However, it should be noted that β-FeOOH NSAs will not be formed if the graphene sheets without β-FeOOH seeds are added in the reaction system (Figure S2, ESI). †In this case, nanorods with nonuniform morphologies are irregularly deposited. Therefore, the presence of β-FeOOH seeds on the surfaces of graphene sheets plays a very important role in the formation of the nanosheet arrays.

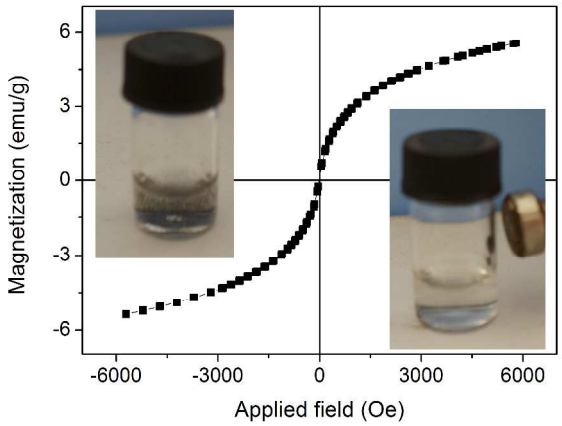

Figure 4 Magnetization hysteresis loop of the 3D G/γ-Fe_2O_3 NSAs, and photographs of the 3D G/magnetic NSAs dispersed in water before (up inset) and after (bottom inset) adding a magnet.

.3. Synthesis of 3D G/γ-Fe_2O_3 NSAs

It is apparent from the inset images in Figure 4 that the 3D G/γ-Fe_2O_3 NSAs, when dispersed in water, can be manipulated by an external magnet. The field-dependent magnetization for the 3D G/γ-Fe_2O_3 NSAs was measured by a VSM at room temperature, as shown in Figure 4. The magnetization hysteresis loop is sigmoidal and the corresponding maximum saturation magnetization value is about 5.47 emu g^{-1}. Since the coercivity and retentivity values are very close to zero, the 3D G/γ-Fe_2O_3 NSAs exhibit a paramagnetic behaviour.

All diffraction peaks indicated by Miller indices in the XRD pattern of G/γ-Fe_2O_3 NSAs can be indexed to cubic maghemite (JCPDS card number 39-1346, cell parameters: a = 8.35 Å) (Figure S3, ESI). † In the Fe 2p core level XPS spectrum of the G/γ-Fe_2O_3 NSAs there are the two main peaks located at 712.4 and 725.3 eV corresponding to Fe 2p3/2 and Fe 2p1/2, respectively (Figure S4, ESI). † The shakeup satellite peak (indicated by the arrow), which is the "fingerprint" of the specific electronic structure of iron oxides such as hematite or maghemite, can be identified.[41] These results imply that the Fe_3O_4 phase is not present in the 3D G/γ-Fe_2O_3 NSAs. The Raman spectrum (Figure S5) shows the characteristic peaks of γ-Fe_2O_3 at 390, 490, and 589 cm^{-1}, while the characteristic peak of magnetite at 668 cm^{-1} is not present.[42] † Thus, the XRD, Raman, and XPS

measurements demonstrate that the magnetic properties of the 3D G/γ-Fe_2O_3 NSAs can be attributed to the presence of γ-Fe_2O_3 in the nanostructures.

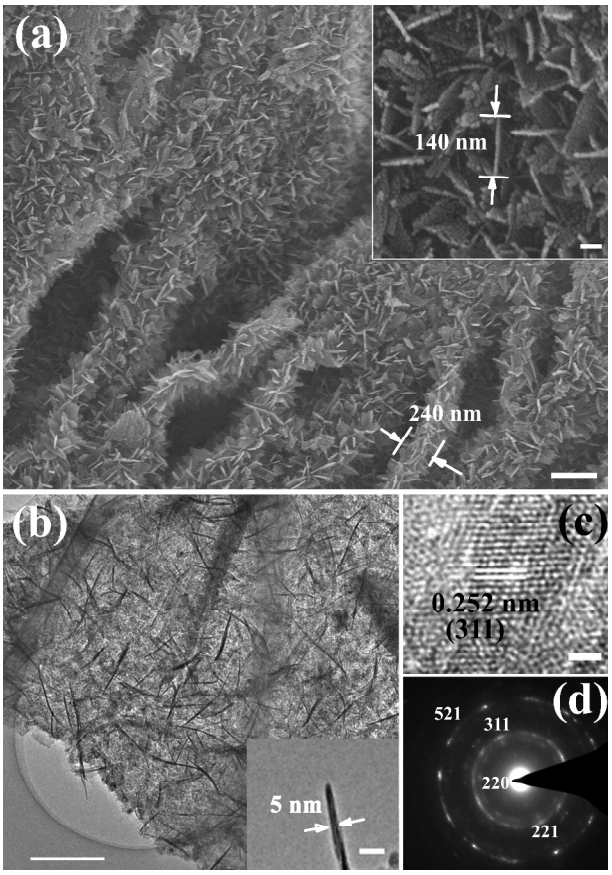

Figure 5 Structural characterization of 3D G/γ-Fe_2O_3 NSAs. (a) SEM image, inset showing magnified top-view SEM image, (b) low-resolution TEM image, (c) HRTEM image for magnetic nanosheets, and (d) SAED pattern. Scale bar: (a) 400 nm, and the inset image: 50 nm, (b) 200 nm, and the inset image: 20 nm, and (c) 2 nm.

The morphology and structure of the 3D G/γ-Fe_2O_3 nanosheet heteronanostructures were further investigated by SEM and TEM measurements. A top-view SEM image, shown in Figure 5(a), indicates that γ-Fe_2O_3 NSAs retained a similar morphology to that of the β-FeOOH NSAs (Figure 3 (a)). The height of the γ-Fe_2O_3 NSAs on the graphene sheets is about 120 nm (Figure 5(a)). The inset in Figure 5(a) is a magnified SEM image, showing that the length of the nanosheets is about 140 nm. The low-resolution and magnified TEM images (Figure 5(b), and inset) demonstrate that the thickness of β-FeOOH nanosheets is about 5 nm. This reveals that, although the 3D nanostructures are similar in overall morphology to those without thermal treatment, the length and the thickness of the nanosheets decreased slightly during thermal treatment. This is a result of structural change of the orthorhombic β-FeOOH to maghemite and the loss of water. Clear lattice fringes are observed in an HRTEM image of the γ-Fe_2O_3 nanosheets (Figure 5(c)), further confirming their crystalline nature. The labeled spacing in the image is about 0.252 nm, corresponding to (311) plane of cubic maghemite. The diffraction rings in the SAED pattern (Figure 5(d)) correspond to (220), (221), (311), and (521) crystalline planes of cubic maghemite. The Bruanuer–Emmett–Teller (BET) surface area of the 3D G/γ-Fe_2O_3 NSAs was calculated to be 113.7 m^2 g^{-1} in terms of the nitrogen adsorption–desorption isotherms (Figure S6, ESI). Collectively, the measurements presented above demonstrate that 3D G/γ-Fe_2O_3 NSAs with paramagnetic properties and high surface area can be fabricated by the seed method.

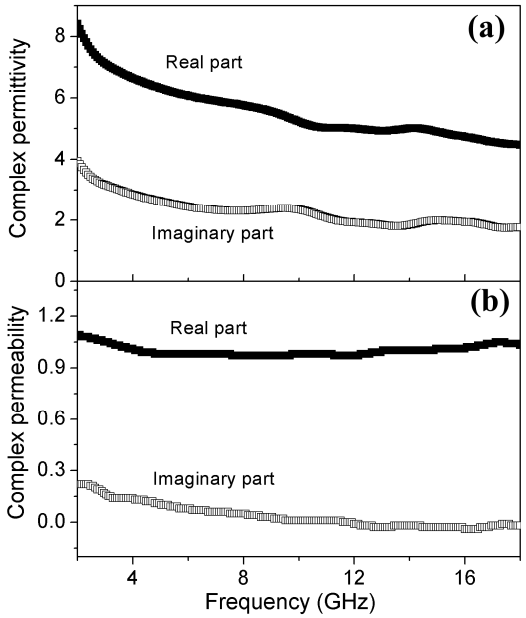

Figure 6 (a) The complex permittivity and (b) the complex permeability of the 3D G/γ-Fe_2O_3 NSAs.

3.4. EM absorption properties of 3D G/γ-Fe_2O_3 NSAs

The EM absorption property of 3D G/γ-Fe_2O_3 NSAs were investigated in terms of the relative complex permittivity ($\varepsilon_r = \varepsilon' - j\varepsilon''$) and the relative complex permeability ($\mu_r = \mu' - j\mu''$). Figure 6(a) shows frequency-dependent relative complex permittivtity curves of the 3D G/γ-Fe_2O_3 NSAs. The real part and the imaginary part vary in the range of 4.5–8.4 and 1.8–4.0, respectively, for the 3D G/γ-Fe_2O_3 NSAs in the frequency region 2–18 GHz. The values of the dielectric loss tangent ($\tan\delta_e = \varepsilon''/\varepsilon'$) of the 3D G/γ-Fe_2O_3 NSAs are 0.36–0.47 over 2–18 GHz (Figure S7, ESI). † These values are significantly larger than those of other magnetic materials.[25, 26] In addition, the dielectric tangent losses fluctuate little over the 2–18 GHz range, which demonstrates that the dielectric loss to EM waves of the 3D G/γ-Fe_2O_3 NSAs is not only strong, but also very stable over this frequency range. Figure 6(b) shows the frequency-dependent relative complex permeability curves of the 3D G/γ-Fe_2O_3 NSAs. The values of the real part are in the range of 0.97–1.09. The weak resonance peak at about 2.0 GHz is similar to the behaviour of G/Fe_3O_4 nanohybrids.[26] The maximum value of the magnetic loss tangent ($\tan\delta_m = \mu''/\mu'$) of the 3D G/γ-Fe_2O_3 NSAs is 0.22, indicating that they present magnetic losses to EM waves. (Figure S7, ESI). †

The 3D G/γ-Fe_2O_3 NSAs have strong and efficient dielectric loss over a 2–18 GHz frequency range which, together with the magnetic loss at low frequencies, suggests that they have good EM absorption properties. The reflection loss (R_L) values were calculated using the following equations at a given frequency and layer thickness according to the transmission line theory: [49]

$$Z_{in} = Z_0(\mu_r / \varepsilon_r)^{1/2} \tanh[\, j(2\pi f d / c)(\mu_r \varepsilon_r)^{1/2} \quad (1)$$

$$R_L = 20\log\left|\frac{(Z_{in} - Z_0)}{Z_{in} + Z_0}\right| \quad (2)$$

In Equations 1 and 2, Z_0 is the impedance of free space, Z_{in} is the input characteristic impedance at the absorber/air interface, c is the velocity of EM waves in free space, f is the frequency of the microwaves, and d is the thickness of the absorber.

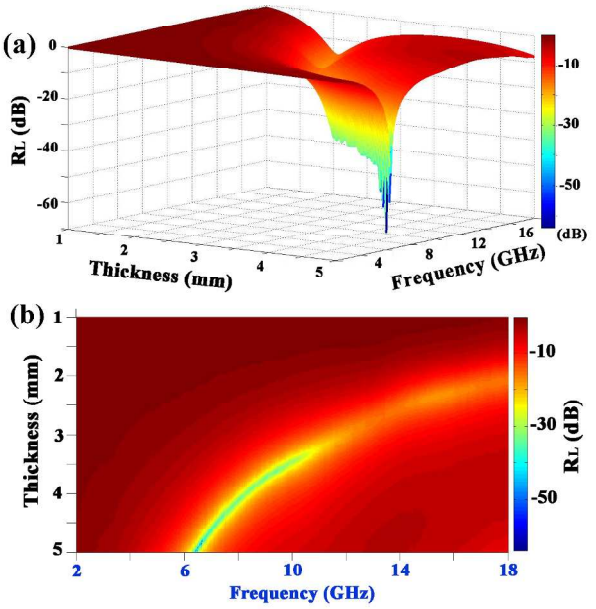

Figure 7 (a) The reflection losses of the 3D G/γ-Fe_2O_3 NSAs and (b) the top view of (a).

Table 1 Comparison of reflection loss of the 3D G/γ-Fe_2O_3 NSAs with other magnetic materials

Materials	R_L, min (dB)	C (wt%)	Reference
Fe_3O_4/ZnO	-30.0	50	27
Fe_3O_4/TiO_2	-20.6	50	28
Fe_3O_4/SnO_2	-27.4	80	25
Fe_3O_4/C	-27.4	55	29
Graphene	> -11.0	20	8
G/Ni	-13.8	20	10
G/Ni	-17.8	60	11
G/Fe_3O_4	-20.0	20	6b
G/γ-Fe_2O_3	-61.4	20	This work

C denotes the addition amount of the absorbents in the paraffin composites.

The calculated reflection losses (R_L) of the 3D G/γ-Fe_2O_3 NSAs are shown in Figure 7. It can be found that the minimal R_L values are less than –15.2 dB for the 3D G/γ-Fe_2O_3 NSAs with the thicknesses of 2 mm, and this increases up to –64.1 dB at 6.48 GHz at a thickness of 4.92 mm. All of the R_L values for the graphene sheets are larger than –11 dB,[8, 17] indicating that the growth of the γ-Fe_2O_3 NSAs on the graphene sheets significantly enhanced their EM absorption properties. Compared with other magnetic materials, such as G/Fe_3O_4 nanohybrids [6] and Fe_3O_4/TiO_2 and Fe_3O_4/SnO_2 core/shell nanostructures, [25, 28, 34] the 3D G/γ-Fe_2O_3 NSAs exhibit very good EM absorption properties (Table 1). For example, the R_L values of the Fe_3O_4/TiO_2 core/shell nanotubes are larger than –20.6 dB when the thickness is in range 2–5 mm. Compared with other graphene-based magnetic materials such as G/Ni and G/Fe_3O_4 heteronanostructures, the 3D G/γ-Fe_2O_3 NSAs also exhibit better EM absorption properties, as shown in Table1. Moreover, the added weight of these magnetic materials in the matrix is more than 40 wt% of the total.[25, 28] Thus, the 3D G/γ-Fe_2O_3 NSAs represent a lightweight alternative to other EM-absorbing materials.

Recently, mechanisms such as zero reflection and geometrical effects have been proposed to interpret the EM absorption properties of these materials. For zero reflection, in terms of EM wave theory, the relationship $\mu_r = \varepsilon_r$ should be satisfied.[22] However, the permittivity of 3D G/γ-Fe_2O_3 NSAs is much higher than their permeability. Therefore, the EM absorption properties of 3D G/γ-Fe_2O_3 NSAs are not explained by the zero reflection mechanism.

As for the geometrical effect, it occurs when the incident and reflected waves in the absorbers are out of phase by 180°. This effect is strongly dependent on the thickness (t) of absorbers according to[44]

$$t = n\lambda_m / 4\,(n = 1, 3, 5, \ldots) \quad (3),$$

where λ_m = c / [f (|μ_r| |ε_r|)1/2] and |μ_r | and |ε_r | are the moduli of μ_r and εr, respectively. According to the calculated reflection losses of the 3D G/γ-Fe_2O_3 NSAs, the matching frequency (f_m), μ_r, and ε_r are equal to 6.48 GHz, 0.98–0.11j, and 5.98–2.38j, respectively. Substituting these values into the Equation 3, the calculated thickness is equal to 4.59 mm, opposed to the true thickness of 4.92 mm. Therefore, the geometric effect is not account for the good EM absorption properties of the 3D G/γ-Fe_2O_3 NSA materials.

The excellent EM absorption performance of the G/γ-Fe_2O_3 NSAs should be related to their special structure and their synergetic effect. On one hand, the γ-Fe_2O_3 NSAs grown on both sides of the graphene sheets can decrease the resistance of the absorbers. The decreased resistivity (1/σ) will lead to an increase in the dielectric loss according to

$$\varepsilon'' \propto \sigma / 2\pi\varepsilon_0 f \quad (4)$$

In that case, the 3D G/γ-Fe_2O_3 nanosheet arrays can consume more heat energy produced as the absorber is irradiated by EM wave.[17, 45-49] On the other hand, as described previously, the graphene sheets exhibited weak EM absorption properties due to the skin effect, i. e., most of incident EM waves were reflected by the G sheet. The reflected EM waves would be attenuated by γ-Fe_2O_3 NSAs again, and thus the 3D G/γ-Fe_2O_3 NSAs exhibited enhanced EM absorption properties. EM absorption properties that depend on special structure have been observed in other 3D nanostructures.[17, 45-49] In addition, the G/γ-Fe_2O_3 nanosheet interfaces are helpful to the improvement of EM absorption properties because of the existing interfacial polarization.[17, 19-21, 30, 31]

4 Conclusion

3D graphene/γ-Fe_2O_3 NSA heteronanostructures were fabricated by a seed-assisted method, in which the γ-Fe_2O_3 nanosheets with lengths, heights, and thicknesses of about 140, 120, and 5 nm, respectively, were grown on both sides of graphene sheets. The 3D nanostructures exhibit paramagnetic behaviour, excellent EM absorption properties, and low weight. The minimal reflection loss was less than –15.2 dB for 3D graphene/γ-Fe_2O_3 NSAs with the thicknesses of 2 mm, and it was up to −64.1 dB when the thickness was 4.92 mm. The excellent EM absorption performance of 3D graphene/γ-Fe_2O_3 NSAs can be attributed to their special structure. In addition, the synthesis strategy presented here could be an important advance in expanding the use of 3D G/magnetic nanostructures into other application areas.

Acknowledgments

This study was carried out under the assistance of National Natural Science Fund of China (Grant nos. 51272050 and 51302047), and Program for New Century Excellent Talents in University (NECT-10-0049).

Notes and references

[a] *Key Laboratory Superlight Materials and surface technology, Ministry of Education , and College of Materials Science and Chemical Engineering, Harbin Engineering University, Harbin, Heilongjiang, 150001, China. Tel: +86-451-82519754; Email: zhuchunling@hrbeu.edu.cn*

[b] *College of Science, Harbin Engineering University, Harbin 150001, China Fax: 86-451-82519754; Tel: 86-451-82519754; E-mail: chenyujin@hrbeu.edu.cn*

[c] *Key Laboratory for Photonic and Electric Bandgap Materials, Ministry of Education, Harbin Normal University, Harbin, 150025, P. R. China*

† Electronic Supplementary Information (ESI) available: XRD pattern of G/β-FeOOH NSAs, SEM image of the sample obtained as the graphene sheets without β-FeOOH seeds in the reaction system. XRD pattern, XPS spectrum, Raman spectrum, the nitrogen adsorption–desorption isotherms and tangent losses of 3D G/γ-Fe_2O_3 NSAs. See DOI: 10.1039/b000000x/

1 X. F. Xia, Q. L. Hao, W. Lei, W. J. Wang, H. L. Wang and X. Wang, *J. Mater. Chem.*, 2012, **22**, 8314.

2 H. L. Wang, H. S. Casalongue, Y. Y. Liang and H. J. Dai, *J. Am. Chem. Soc,*. 2010, **132**, 7472.

3 H. L. Wang, L. F. Cui, Y. Yang, H. S. Casalongue, J. T. Robinson, Y. Y. Liang, Y. Cui and H. J. Dai, *J. Am. Chem. Soc*. 2010, **132**, 13978.

4 H. K. He, and C. Gao, *ACS Appl. Mater. Interfaces*, 2010, **2**, 3201

5 Y. J. Chen, Q. S. Wang, C. L.Zhu, P. Gao, Q. Y. Ouyang, T. S. Wang, Y. Ma and C. W. Sun, *J. Mater. Chem.,* 2012, **22**, 5924.

6 (a) T. S. Wang, Z. L. Liu, M. M. Lu, B.Wen, Q. Y. Ouyang, Y. J. Chen, C. L. Zhu, P. Gao, C. Y. Li, M. S. Cao and L. H. Qi, *J. Appl. Phys,*. 2013, **113**, 024314. (b) W. D. Xue, R. Zhao, X. Du, F. W. Xu, M. Xu and K. X. Wei, *Mater. Res. Bull.*, 2014, **50**, 285.

7 (a) H. Zhang , A. J. Xie, C. P. Wang, H. S. Wang, Y. H. Shen and X. Y. Tian, *J. Mater. Chem. A.,* 2013, **1**, 8547. (b) M. Zong, Y. Huang, H. W. Wu, Y. Zhao, Q. F. Wang and X. Sun, *Mater. Lett.* 2014, **114**, 52.

8 Y. L. Ren, H. Y. Wu, M. M. Lu, Y. J. Chen, C. L. Zhu, P. Gao, M. S. Cao, C. Y. Li and Q. Y. Ouyang, *ACS Appl. Mater. Interfaces.,* 2012, **4**, 6436.

9 C. G. Hu, Z. Y. Mou, G. W. Lu, N. Chen, Z. L. Dong, M. J. Hua and L. T. Qu, *Phys. Chem. Chem. Phys.*, 2013, **15**, 13038.

10 Y. Cao, Q. M. Su, R. C. Che, G. H. Du and B. S.Xu, *Synthetic Met.,* 2012, **162**, 968.

11 T. T. Chen, F. Deng, J. Zhu, C. F. Chen, G. B. Sun, S. L. Ma and X. J. Yang, *J. Mater. Chem.*, 2012, **22**, 15190.

12 K. Y. Chen, C. Xiang, L. C. Li, H. S. Qian, Q. S. Xiao and F. Xu, *J. Mater. Chem.*, 2012, **22**,6449.

13 (a) D. Y. Chen, G. Ji, Y. Ma, J. Y. Lee and J. M. Lu, *ACS Appl. Mater. Interfaces,* 2011, **3**, 3078. (b) X. H. Jia, H. J. Song, C. Y. Min and X. Q. Zhang, *AppL. Phys. A.*, 2012, **109**, 261. (b) D. Y. Chen, G. Ji, Y. Ma, J. Y. Lee and J. M. Lu, *ACS Appl. Mater. Interfaces,* 2011, **3**, 3078.

14 Q. Y. Ouyang, H. L. Yu, Z. Xu, Y. Zhang, C. Y. Li, L. H. Qi and Y. J. Chen. *Appl. Phys. Lett,*. 2013, **102**, 031912.

15 H. L. Yu, C. Ma, B. H. Ge, Y. J. Chen, Z. Xu, C. L. Zhu, C. Y. Li, Q. Y Ouyang, P. Gao, J. Q. Li, C. W. Sun, L. H. Qi, Y. M. Wang and F. H. Li, *Chem. Eur. J.* 2013, **19**, 5818.

16 A. N. Cao, Z. Liu, S. S. Chu, M. H. Wu, Z. M. Ye, Z. W. Cai, Y. L. Chang, S. F. Wang, Q. H. Gong and Y. F. Li, *Adv. Mater.,* 2010, **22**, 103.

17 H. L. Yu, T. S. Wang, B. Wen, M. M. Lu, Z. Xu, C. L. Zhu, Y. J. Chen, X. Y. Xue, C. W. Sun and M. S. Cao, *J. Mater. Chem.,* 2012, **22**, 21679.

18 B. Liu, J. Zhang, X. F. Wang, G. Chen, D. Chen, C. W. Zhou and G. Z. Shen, *Nano Lett.,* 2012, **12**, 3005.

19 L. J. Deng and M. Han, *Appl. Phys. Lett,*. 2007, **91**, 023119.

20 C. C. Lee and C. H. Chen, *Appl. Phys. Lett,*. 2007, **90**, 193102.

21 R. C. Che, L. M. Peng, X. F. Duan, Q. Chen and X. L. Liang, *Adv. Mater,*. 2004, **16**, 401–405.

22 J. Liu, R. C. Che, H. J. Chen, F. Zhang, F. Xia, Q. S. Wu and M. Wang, *Small*, 2012, 8, 1214.

23 X. G. Liu, D. Y. Geng, H. Meng, P. J. Shang and Z. D. Zhang, *Appl. Phys. Lett.,* 2008, 92, 173117.

24 X. G. Liu, D. Y. Geng and Z. D. Zhang, *Appl. Phys. Lett.,* 2008, **92**, 243110.

25 (a) C. Brosseau, J. B. Youssef, P. Talbot and A. M. Konn, *J. Appl. Phys.,* 2003, **93**, 9243. (b) Y. J. Chen, P. Gao, R. X. Wang, C. L. Zhu, L. J. Wang, M. S. Cao and H. B. Jin, *J. Phys. Chem. C,* 2009, **113**, 10061.

26 Y. J. Chen, M. S. Cao, T. H. Wang and Q. Wan, *J. Appl. Phys.,* 2009, **106**, 054303.

27 (a) F. Qin and C. Brosseau,*J. Appl. Phys.,* 2003, **93**, 9243. (b) Y. J. Chen, F. Zhang, G. G. Zhao, X. Y. Fang, H. B. Jin, P. Gao, C. L. Zhu, M. S. Cao, G. Xiao, *J. Phys. Chem. C,* 2010, 114, 9239.

28 C. L. Zhu, M. L. Zhang, Y. J. Qiao, G. Xiao, F. Zhang and Y. J. Chen, *J. Phys. Chem. C,* 2010, **114**, 16229.

29 Y. J. Chen, G. Xiao, T. S. Wang, Q. Y. Ouyang, L. H. Qi, Y. Ma, P. Gao, C. L. Zhu, M. S. Cao and H. B. Jin, *J. Phys. Chem. C,* 2011, **115**, 13603.

30 J. W. Liu, J. J. Xu, R. C. Che, H. J. Chen, M. M. Liu and Z. W. Liu, *Chem. Eur. J.,* 2013, **19**, 6746.

31 J. W. Liu, J. Cheng, R. C. Che, J. J. Xu, M. M. Liu and Z. W Liu, *J. Phys. Chem. C,* 2013, **117**, 489.

32 J. J. Liang, Y. Wang, Y. Huang, Y. F. Ma, Z. F. Liu, J. M. Cai, C. D. Zhang, H. J. Gao and Y. S. Chen, *Carbon,* 2009, **47**, 922.

33 X. Bai, Y. H. Zhai and Y. Zhang, *J. Phys. Chem. C*, 2011, **115**, 11673.

34 C. Wang, X. J. Han, P. Xu, X. L. Zhang, Y. C. Du, S. R. Hu, J. Y. Wang and X. H. Wang, *Appl. Phys. Lett.,* 2011, **98**, 072906.

35 Y. L. Ren, C. L. Zhu, S. Zhang, C. Y. Li, Y. J. Chen, P. Gao, P. P. Yang and Q. Y. Ouyang, *Nanoscale*,2013, **5**, 12296.

36 C. M. Ban, Z. C. Wu, D. T. Gillaspie, L. Chen, Y. F. Yan, J. L. Blackburn and A. C. Dillon, *Adv. Mater.,* 2010, **22**, E145.

37 J. P. Liu, Y. Y. Li, H. J. Fan, Z. H. Zhu, J. Jiang, R. Ding, Y. Y. Hu and X. T. Huang, *Chem. Mater.,* 2010, **22**, 212.

38 Y. J. Chen, F. N. Meng, C. Ma, Z. W. Yang, C. L. Zhu, Q. Y. Ouyang, P. Gao, J. Q. Li and C. W. Sun, *J. Mater. Chem.,* 2012, **22**, 12900.

39 Y. J. Chen, X. M. Gao, X. P. Di, Q. L. Ouyang, P. Gao, L. H. Qi, C. Y. Li and C. L. Zhu, *ACS Appl. Mater. Interfaces,* 2013, **5**, 3267.

40 Y. J. Chen, Z. Y. Lei, H. Y. Wu, C. L. Zhu, P. Gao, L. H. Qi, Q. L. Ouyang and W. Qin, *Mater. Res. Bull.,* 2013, **48**, 3362.

41 T. Fujii, F. M. F. de Groot, G. A. Sawatzky, F. C. Voogt, T. Hibma and K. Okada, *Phys. Rev. B,* 1999, **59**, 3195.

42 D. L. A. de Faria, S. Venâncio Silva and M. T. de Oliveira, *J. Raman Spectrosc.* 1997, **28**, 873.

43 S. S. Kim, S. B. Jo, K. K. Choi, J. M. Kim, K. S. Churn, *IEEE Trans. Magn*., 1991, **27**, 5462.

44 A. N. Yusoff, M. H. Abdullah, S. H. Ahmad, S. F. Jusoh, A. A. Mansor and S. A. A. Hamid, *J. Appl. Phys*., 2002, **92**, 876.

45 G. B. Sun, B. X Dong , M. H. Cao, B. Q. Wei and C. W. Hu, *Chem. Mater.* 2011, **23**, 1587.

46 Q. S. Wang, Z. Y. Lei, Y. J. Chen, Q. Y. Ouyang, P. Gao, L. H. Qi, C. L. Zhu and J. Z. Zhang, *J. Mater. Chem. A*, 2013, **1**, 11795.

47 M. Zhou, X. Zhang, J. M. Wei, S. L. Zhao, L. Wang and B. X. Feng, *J. Phys. Chem. C*, 2011, **115**, 1398.

48 H. Wen, M. H. Cao, G. B. Sun, W. G. Xu, D. Wang, X. Q. Zhang and C. W. Hu, *J Phys Chem C*., 2008, **112**, 15948.

49 R. F. Zhou, H. T. Feng, J. T. Chen, D. Yan, J. J.Feng, H. J. Li, B. S. Geng, S. Cheng, X. Y. Xu and P. X. Yan, *J. Phys. Chem. C*, 2008, **112**, 11767.